

# Effects of Cooling Rate on Transformations in a Fe-9 Pct Ni Steel

RICHARD W. FONDA and GEORGE SPANOS

The transformations of a high-strength 9Ni-Cr-Mo-V steel were characterized as a function of cooling rate by dilatometry, microhardness measurements, and microstructural characterization. The results demonstrate that this steel is extremely insensitive to changes in cooling rate, generating a duplex microstructure of coarse autotempered martensite within a matrix of fine lath martensite at nearly all cooling rates. The coarse autotempered martensite is observed even at very slow cooling rates, although the lath martensite becomes replaced by lath (or bainitic) ferrite.

DOI: 10.1007/s11661-014-2588-3

© The Minerals, Metals & Materials Society and ASM International 2014

## I. INTRODUCTION

NEW high-strength steels with good toughness and corrosion resistance have long been in demand for Naval ship construction.<sup>[1-6]</sup> However, concurrently attaining high levels of both strength and toughness in an alloy are often difficult, as the toughness of high-strength steels is usually limited. It has long been known<sup>[7,8]</sup> that increasing the Nickel content of steels will both increase the strength and dramatically lower the transition temperature. Speich *et al.*<sup>[9]</sup> observed that additions of Co and Mo to high-nickel steels can increase their strength while retaining their toughness, which led to the development of high-Co, high-Ni steels such as AF1410 (14Co-10Ni-2Cr-1Mo-0.16C)<sup>[10,11]</sup> and Aermet 100 (13.4Co-11.1Ni-3.1Cr-1.2Mo-0.23C).<sup>[12]</sup> The high nickel content of these high-strength steels contributes to their good toughness, presumably through promoting cross slip and thus higher strain hardening, while the cobalt increases the hardness and yield strength, particularly at higher tempering temperatures.<sup>[9]</sup> The current 9Ni-Mo-Cr-V high-strength steel arose from an analysis of the effects of the various alloying elements in these steels. This Co-free steel has a lower (0.11 pct) carbon level, but can be thermally processed to achieve a high yield strength (160 ksi) and a toughness [ $C_v$  impact values as high as 120 ft-lbs at 78 K (−195 °C)] that surpasses that of many currently available ultra-high-strength steels, while exhibiting an excellent stress corrosion cracking resistance in sea water.<sup>[13,14]</sup>

The development of new steels for Naval application requires an understanding of their transformation behavior across a range of cooling rates to anticipate the variations that could result from production varia-

tions and construction processes such as welding. Continuous cooling transformation (CCT) diagrams are a convenient illustration of the phase transformation behavior of a material as a function of cooling rate.<sup>[15]</sup> CCT diagrams show the microstructures produced at different cooling rates, and thus provide a predictive indicator of the mechanical properties that will result from comparable thermal cycles, such as would occur during conventional thermal processing or welding. CCT diagrams are therefore useful both to define the desired range of cooling rates to achieve a specific microstructure and to indicate the microstructures that can result from deviations outside of those desired cooling rates. The ultimate purpose of this study was thus to determine the transformation characteristics and develop a CCT diagram for this new 9 pct Ni steel of interest for naval and other high-strength applications.

## II. EXPERIMENTAL

The alloy examined in this study is a low carbon (0.11 wt pct), 9Ni-Cr-Mo-V steel with compositional levels typical of the alloys described in the US patent #4,814,141.<sup>[13]</sup> Specimens measuring 3.0 mm in diameter and 10 mm in length were machined from the base plate along the rolling direction. These specimens were heated in an MMC heating/quenching dilatometer at a rate of 300 °C/min to a temperature of 1473 K (1200 °C), where they were held for 4 minutes. The samples were then cooled at various rates ranging from approximately  $\Delta t_{8/5} = 1$  second to  $\Delta t_{8/5} = 10,000$  seconds (cooling rates of 130 °C/s to 0.016 °C/s) with “natural cooling”, in which the cooling rate is proportional to the temperature difference between the sample and its surroundings. The parameter  $\Delta t_{8/5}$  is the time taken by the sample to cool down from 1073 K to 773 K (800 °C to 500 °C); a smaller  $\Delta t_{8/5}$  corresponds to a faster cooling rate, and vice versa. The reported cooling rate (CR) for each sample corresponds to a linear cooling rate measured immediately above the transformation

RICHARD W. FONDA, Head of Microstructural Evolution and Joining Section, is with the Naval Research Laboratory, Washington, DC. Contact e-mail: Richard.Fonda@nrl.navy.mil GEORGE SPANOS, formerly with the Naval Research Laboratory, is now Technical Director with The Minerals, Metals, & Materials Society (TMS), Warrendale, PA. Manuscript submitted October 8, 2013.

Article published online October 2, 2014

start temperature [approximately 623 K (350 °C)] since the cooling rate of each sample varies with temperature during the natural cooling process. External cooling with helium was used to achieve the cooling rates with  $\Delta t_{8/5} \leq 32$  seconds (CR  $\geq 2$  °C/s). From the resultant dilatation vs temperature curves, the transformation start (1 pct transformation) and finish (99 pct transformation) temperatures were calculated by standard procedures<sup>[15]</sup> for use in construction of the CCT diagram.

Additional dilatometry was also performed to better understand the overall transformation behavior, particularly during continuous heating and isothermal heat treatments. The continuous heating experiments were conducted at constant heating rates ranging from 1 to 300 °C/min. The isothermal experiments were performed by heating the sample at 300 °C/min to a temperature from 823 K to 1023 K (550 °C to 750 °C), maintaining the specimen at that temperature for 60 minutes, and then continuing to heat the specimen, again at a heating rate of 300 °C/min, to a final temperature of at least 1173 K (900 °C), exceeding the transformation finish temperature.

The dilatometry specimens were analyzed by optical microscopy, scanning electron microscopy (SEM), transmission electron microscopy (TEM), and microhardness measurements in addition to the standard dilatometric analysis. Optical microscopy and SEM were performed after standard metallographic polishing and etching with a 2 pct Nital solution. TEM analyses were performed on thin disks sliced from the dilatometry specimens which were mechanically thinned to about 50  $\mu\text{m}$ , dimpled, and then electropolished on a Fischione twin-jet electropolisher at room temperature (to retain any untransformed austenite that may be present) with a solution of 100 g anhydrous sodium chromate in 500 mL glacial acetic acid at 55 to 60 V, corresponding to approximately 25 mA. The SEM samples were analyzed on a JEOL JSM-7001F SEM operating at 20 kV while the TEM samples were analyzed on a Philips CM30 TEM operating at 300 kV. Microhardness testing was performed with a Vickers indenter and a 1000 g load. Each microhardness value reported here is the average of 7 measurements taken at 0.8 mm separation.

### III. RESULTS AND DISCUSSION

#### A. Dilatometry and Microhardness

The transformation temperatures exhibited by this Fe-9Ni-Cr-Mo-V steel during cooling were determined by dilatometry across a wide range of cooling rates. Throughout most of this cooling rate regime, however, the transformation temperatures remain nearly constant (see Figure 1). Other than the surface cooling effects and other experimental artifacts present at the fastest cooling rates, this alloy exhibits a transformation start temperature of approximately 603 K (330 °C) and a transformation finish temperature of approximately 453 K (180 °C) for all cooling rates with  $\Delta t_{8/5} \leq 994$  seconds

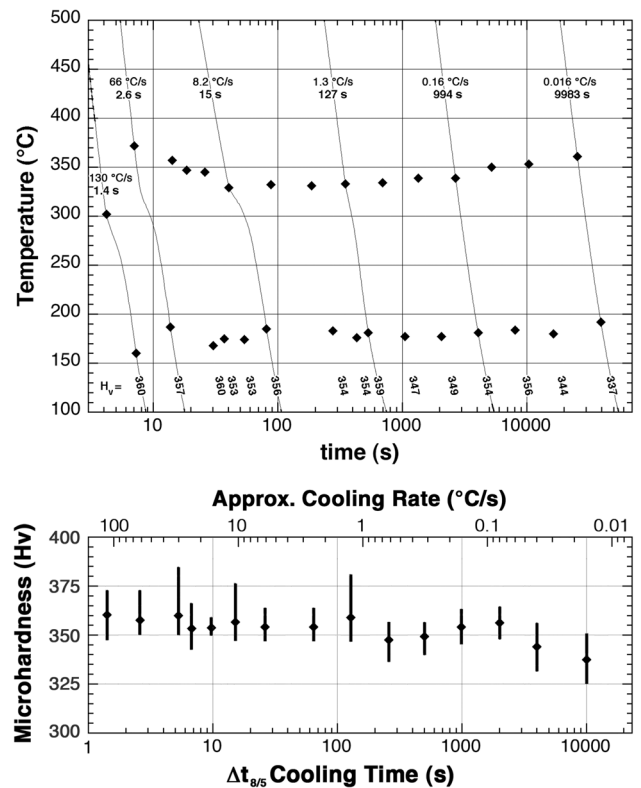


Fig. 1—Transformation temperatures, Vickers microhardness, and selected cooling curves of the steel samples shown as a function of cooling rate.

(CR  $\geq 0.16$  °C/s). This reflects a very high hardenability for this alloy, indicating that it is very forgiving to changes in thermal processing or welding conditions. At even slower cooling rates ( $\Delta t_{8/5} \geq 1991$  seconds or CR  $\leq 0.085$  °C/s), the transformation start temperature is slightly higher, which is usually indicative of a ferritic transformation. These temperatures are lower than those exhibited by the near-binary Fe-0.002C-9.14Ni alloy, which has a  $\sim 50$  °C higher martensite start temperature and a more than 100 °C higher ferritic transformation start temperature.<sup>[16]</sup> On the other hand, the transformation in this Fe-0.11C-9Ni-Cr-Mo-V steel is about 100 °C higher than in the high-cobalt AerMet 100 alloy.<sup>[17]</sup>

All of the observed transformations occur well below the  $T_0$  temperature in this alloy. The  $T_0$  temperature is the temperature at which metastable austenite and metastable ferrite of the same composition are in a metastable equilibrium; austenite is more stable than ferrite or martensite at temperatures above  $T_0$ , while ferrite and martensite are more stable at temperatures below  $T_0$ . The  $T_0$  temperature can be estimated as the average of the temperatures required to produce the same fraction of product for the  $\alpha \rightarrow \gamma$  transformation and  $\gamma \rightarrow \alpha$  reverse transformation.<sup>[18]</sup> For this alloy, dilatometry measurements during heating and cooling show that 50 pct transformation during cooling occurs at 573 K (300 °C) while 50 pct transformation during heating occurs at 1023 K (750 °C), leading to an estimated  $T_0$  temperature of 798 K (525 °C). This is

approximately 100 °C below the  $T_0$  temperature of the binary Fe-9 pct Ni alloy,<sup>[18]</sup> as reflected in the transformation temperatures discussed above.

The transformation temperatures of this alloy can also be estimated using empirical transformation temperature models. Although the high nickel content of the current steel is outside the compositional range for these models, it is useful to compare the observed transformation temperatures to the predictions of those formulas. The formulas developed by Andrews<sup>[19]</sup> predict an  $M_s$  temperature of about 573 K (300 °C), slightly below the observed  $M_s$  temperature of 603 K (330 °C). The predicted  $B_s$  temperature,<sup>[20]</sup> however, is approximately 553 K (280 °C), below both the predicted  $M_s$  temperature and the observed transformation temperature, indicating that the expected transformation product is martensitic.

The microhardness of an alloy can provide an indication of the mechanical properties, particularly the yield strength, of that alloy.<sup>[21]</sup> The variation in microhardness of this alloy as a function of cooling rate is shown in Figure 1. This figure demonstrates that the microhardness remains nearly constant throughout most of the cooling rates examined, suggesting that the predominant microstructure is maintained through all these cooling rates. The only significant variation is a slight decrease in microhardness observed for the two extremely slow cooling rates with  $\Delta t_{8/5} = 3891$  and 9983 seconds (CR = 0.041 and 0.016 °C/s). These microhardness trends are consistent with the microstructural observations (see below).

The transformation behavior upon heating was also determined by dilatometry as a function of heating rate (Figure 2(a)). At the fastest heating rates, corresponding to 100 and 300 °C/min, the transformation start temperature ( $A_{c1}$ ) was measured to be about 968 K (695 °C) and the transformation finish temperature ( $A_{c3}$ ) was about 1073 K (800 °C). The  $A_{c1}$  decreases to 888 K (615 °C) at 25 °C/min and then to 868 K (595 °C) for even slower rates, indicating a partial (at 25 °C/min) or complete (at 5 and 1 °C/min) dissolution of the carbide precipitates and commensurate enrichment of carbon in the matrix. The  $A_{c3}$  did not exhibit any significant deviations.

Isothermal heat treatments (Figure 2(b)) were also conducted to determine the equilibrium transformation start and finish temperatures,  $A_{e1}$  and  $A_{e3}$ . The results of these experiments revealed that the transformation begins at approximately 823 K (550 °C) and is fully complete just below 973 K (700 °C), supporting previous estimates of those transformation temperatures.<sup>[22]</sup> These temperatures are similar to the  $A_{e1}$  and  $A_{e3}$  temperatures calculated from the formulas presented by Grange<sup>[23]</sup> and Andrews,<sup>[19]</sup> which predict  $A_{e1}$  temperatures of about 863 K and 843 K (590 °C and 570 °C) and  $A_{e3}$  temperatures of 933 K and 993 K (660 °C and 720 °C), respectively.

## B. Microstructures

The initial microstructure of this steel consists of a bands of polygonal ferrite embedded in a matrix of fine acicular laths, as shown in Figure 3. This initial micro-

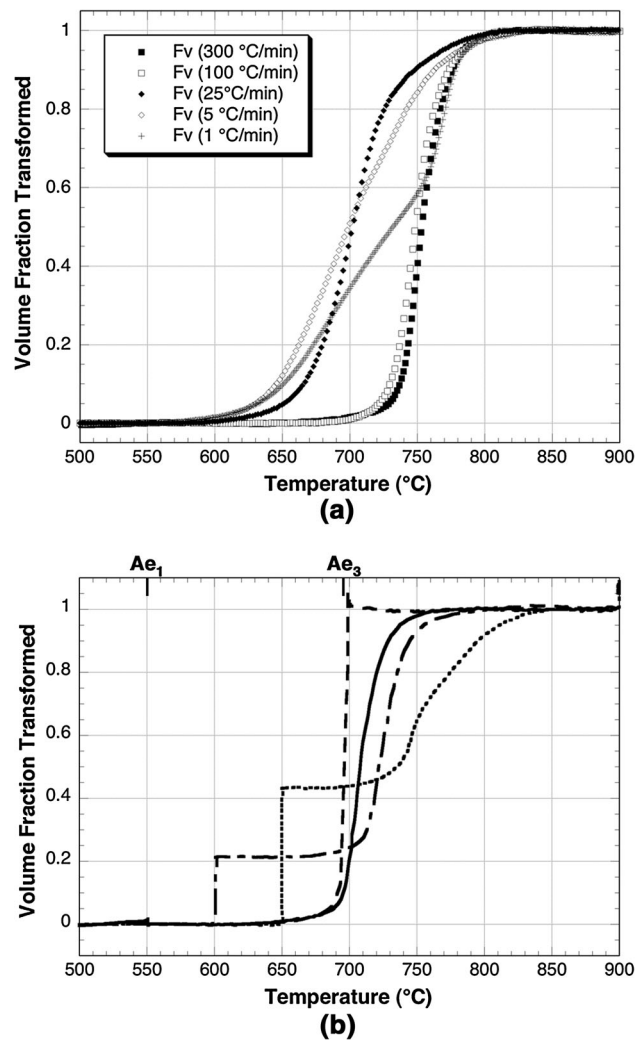


Fig. 2—Dilatometry showing the formation of austenite during (a) continuous and (b) isothermal heating of the steel. The  $A_{c1}$  and  $A_{c3}$  temperatures in Fig. 2(a) correspond to the transformation start (1 pct transformation) and finish (99 pct transformation) temperatures, respectively.

structure is fully transformed during the austenitization heat treatment prior to cooling, obscuring any remnant of this structure in the heat-treated samples discussed below.

The observed uniformity of transformation behavior as a function of cooling rate is consistent with the similarity among the optical micrographs of the resultant microstructures (Figure 4). The microstructures appear nearly constant throughout a wide range of cooling rates from the fastest cooling rates through cooling rates as slow as  $\Delta t_{8/5} = 994$  s, or 0.16 °C/s (see Figures 4(a) through (e)). These microstructures appear to be fully martensitic, consisting of coarse martensite constituents that often exhibit a characteristic flat end on one side and a tapered end on the other<sup>[24–26]</sup> and are embedded within a matrix of fine lath martensite that cannot be well resolved due to the resolution limitations of optical microscopy. The size, morphology, and proportions of these constituents do not vary significantly as a function of cooling rate, although an

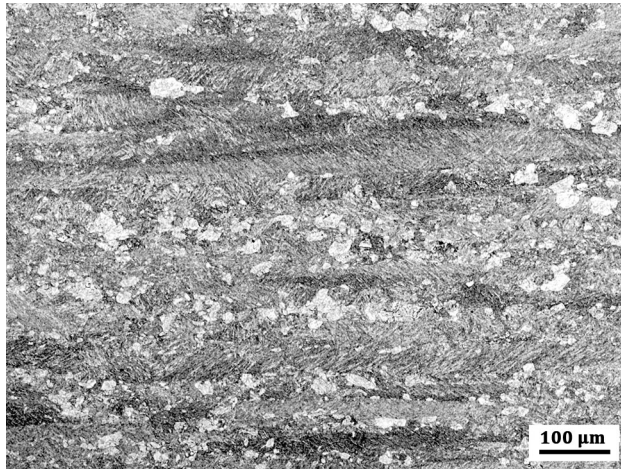


Fig. 3—Optical micrograph of the microstructure of the as-received base plate.

increase in prior austenite grain size is evident at slower cooling rates, reflecting the longer time spent at elevated temperatures for those samples.

Electron microscopy was used to reveal the finer details of these microstructures. Both SEM (Figure 5) and TEM (Figure 6) confirm that all fast to moderately slow cooling rates produce a similar microstructure consisting of a coarse martensite constituent in a matrix of fine lath martensite. Previous complimentary direct quench and temper and continuous cooling studies have demonstrated that the coarse microstructure is a martensitic microconstituent,<sup>[24–26]</sup> although it has been referred to more recently as coalesced bainite.<sup>[27–29]</sup> The TEM observations indicate that except at the very slowest cooling rates, the fine lath microstructure exhibits significant crystallographic misorientations between laths (*i.e.*, adjacent fine lath constituents exhibit significant contrast variations) with straight interlath boundaries often coated with thin layers of retained austenite. These observations are characteristic of fine lath martensite.<sup>[30]</sup>

The primary microstructural differences resulting from these cooling rates are in the prominence of the fine lath boundaries and the extent of the autotempered cementite precipitation within the coarse martensite. Despite the low transformation temperature exhibited by this alloy, cementite platelets precipitate within the larger martensite constituents during cooling in a process known as autotempering.<sup>[31]</sup> At the fastest cooling rate ( $\Delta t_{8/5} = 1.4$  seconds or CR = 130 °C/s), the coarse martensite is nearly devoid of these internal cementite precipitates; nascent cementite precipitates are barely visible by TEM (Figure 6(a)). Slower cooling rates, however, clearly exhibit the characteristic multiple variants of autotempered cementite precipitates within the coarse martensite. Fine, autotempered cementite precipitates are present in the coarse martensite phase that forms at  $\Delta t_{8/5} = 2.6$  seconds (66 °C/s), and those precipitates coarsen as the cooling rate is decreased. The three cementite variants in this autotempered martensite are indicated in the inset images in Figures 6(b) through (d). Thus, while there is insufficient time for cementite to

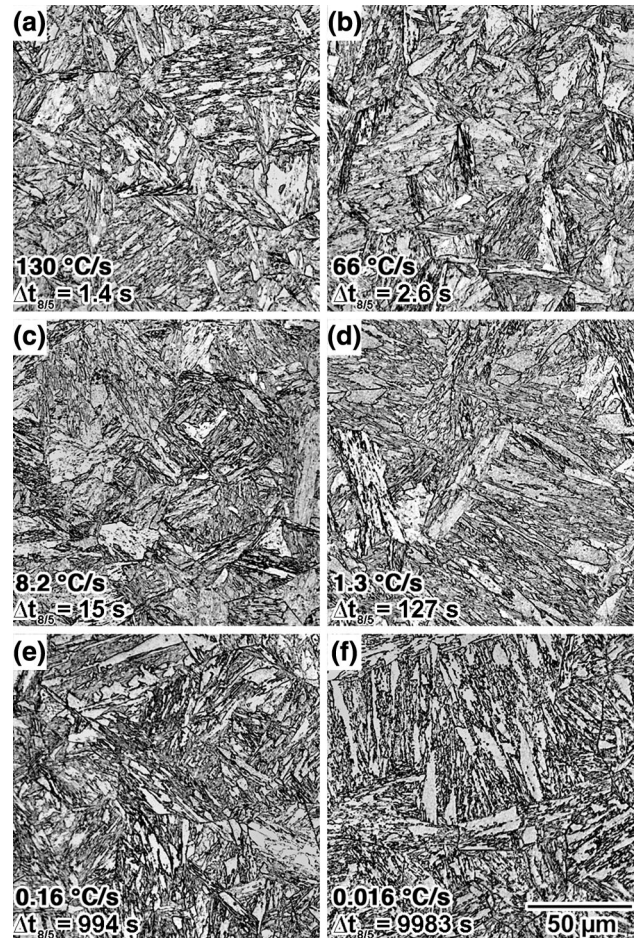


Fig. 4—Optical micrographs showing the variation in microstructure as a function of cooling rate. (a)  $\Delta t_{8/5} = 1.4$  s (130 °C/s), (b)  $\Delta t_{8/5} = 2.6$  s (66 °C/s), (c)  $\Delta t_{8/5} = 15$  s (8.2 °C/s), (d)  $\Delta t_{8/5} = 127$  s (1.3 °C/s), (e)  $\Delta t_{8/5} = 994$  s (0.16 °C/s), and (f)  $\Delta t_{8/5} = 9983$  s (0.016 °C/s).

precipitate during cooling at the fastest cooling rate, multiple variants of cementite are evident within the coarse martensite at all other cooling rates.

The coarse constituent observed in this study was identified as a coarse martensite, in accord with previous studies.<sup>[24–26,32,33]</sup> However, more recent publications by Bhadeshia *et al.*<sup>[27–29]</sup> have referred to similar microstructures as coalesced bainite. One of the primary reasons to identify this as martensite is that the same microstructure can also be produced by a rapid quench and temper experiment. For example, rapidly quenching an HSLA-100 sample from 1573 K (1300 °C) into ice brine, which precludes possible diffusional transformations such as bainite, produces an essentially identical coarse morphology, and subsequent tempering replicates the multiple cementite variants observed in this constituent.<sup>[24]</sup> The presence of multiple (typically three) cementite orientation variants in each crystal also suggests that this constituent initially formed as a supersaturated component and that the precipitation of cementite occurs during subsequent cooling unless the supersaturation is quenched in through a very fast cooling rate. The complex morphology of this constit-

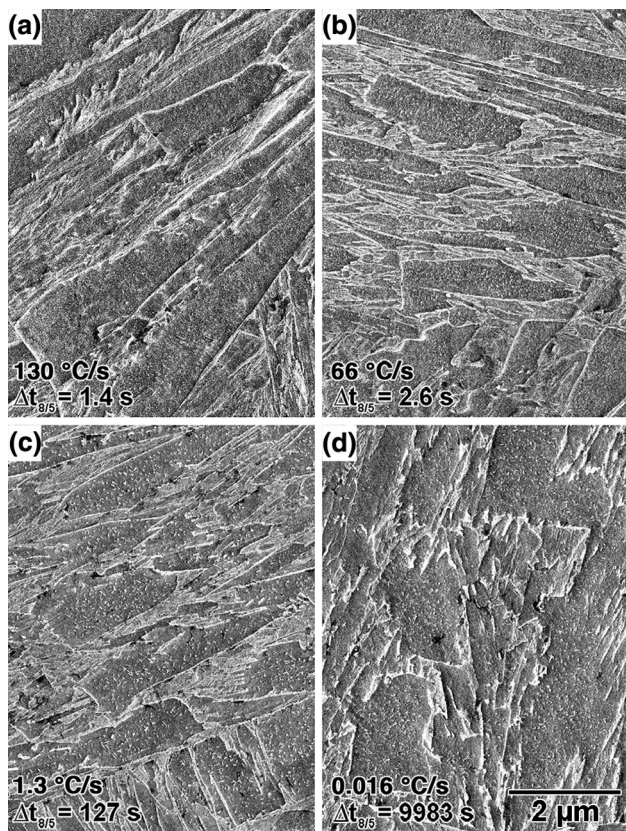


Fig. 5—SEM images of the microstructure as a function of cooling rate. (a)  $\Delta t_{8/5} = 1.4$  s (130 °C/s), (b)  $\Delta t_{8/5} = 2.6$  s (66 °C/s), (c)  $\Delta t_{8/5} = 127$  s (1.3 °C/s), and (d)  $\Delta t_{8/5} = 9983$  s (0.016 °C/s).

uent can also exhibit regions that appear consistent with the coalescence of the martensite laths, indicating the need for further research into this coarse martensite constituent.

The two slowest cooling rates examined in this study ( $\Delta t_{8/5} = 3981$  seconds (0.041 °C/s) and  $\Delta t_{8/5} = 9983$  seconds (0.016 °C/s), shown in Figure 4(f)) also generate a bimodal-sized microstructure, although the fine scale constituent boundaries appear significantly rougher or more undulated by optical microscopy. The coarse constituents are similar in size, shape, and number to those observed at faster cooling rates, even exhibiting the characteristic flat end in many cases. The rough or undulated appearance of the fine lath boundaries suggests a more ferritic or bainitic microstructure. The sample cooled at  $\Delta t_{8/5} = 1991$  seconds (0.085 °C/s) has an intermediate appearance between this microstructure and the martensitic microstructures formed at faster cooling rates. While a significant fraction of the constituent boundaries exhibit cleaner or more linear features similar to those observed at the faster cooling rates, a majority exhibit the roughness characteristic of the slower cooling rates.

Electron microscopy of the microstructures that develop at the slowest cooling rates (Figures 5(d) and 6(d)) reveal similar coarse constituents but different fine lath constituents as compared to the microstructures

that develop at faster cooling rates. The coarse martensite not only exhibits a similar morphology, but also contains the multiple cementite variants typical of the autotempered coarse martensite constituents formed at faster cooling rates. On the other hand, the fine lath structure surrounding the coarse components is distinctly different. This fine lath structure (see Figures 6(d) and 7) has a much more uniform gray color with low contrast between adjacent laths, indicating a similar crystallographic orientation of the laths within a packet. The interlath boundaries also have a curved or wavy appearance and the retained austenite between the laths has a more blocky appearance, consistent with a lath ferrite (or bainitic ferrite) microstructure.<sup>[30]</sup> Thus, this microstructure is consistent with coarse martensite constituents embedded within a matrix of lath or bainitic ferrite.

### C. Continuous Cooling Transformation Diagram

The dilatometry, microhardness, and microstructure results just described were compiled and integrated to produce the CCT diagram shown in Figure 8. This CCT diagram demonstrates the extreme insensitivity to changes in the cooling rate exhibited by this alloy.

At nearly all of the cooling rates examined, ranging from the fastest cooling rate with  $\Delta t_{8/5} = 1.4$  seconds (130 °C/s) to a slow cooling rate with  $\Delta t_{8/5} = 994$  seconds (0.16 °C/s), the austenite transforms to a fully martensitic microstructure characterized by coarse autotempered martensite within a matrix of fine lath martensite. While only a few small autotempered cementite precipitates were observed within the coarse martensite at the fastest cooling rates ( $\Delta t_{8/5} < \sim 2$  seconds,  $CR > \sim 100$  °C/s), those precipitates rapidly increase in size and number as the cooling rate is decreased and are prevalent through most of the cooling rates examined. The microhardness obtained from these cooling rates is also relatively constant, decreasing only slightly (from 360 to 350 HV) across this wide range of cooling rates, reflecting the uniformity of the reaction products generated through this range of cooling rates.

At very slow cooling rates (those with a  $\Delta t_{8/5}$  of at least 994 seconds or  $CR \leq 0.16$  °C/s), the coarse autotempered martensite constituent is still observed but the fine structure surrounding it develops into a predominantly ferritic/bainitic microstructure. At  $\Delta t_{8/5} = 1991$  seconds (0.085 °C/s), the fine constituents comprised both lath martensite and lath (or bainitic) ferrite, and then become fully ferritic/bainitic at the two slowest cooling rates.

The CCT diagram for this 9Ni-Mo-Cr-V high-strength steel bears a strong resemblance to the Carpenter AerMet 100 alloy.<sup>[17]</sup> Both alloys exhibit a very high hardenability producing a lath martensitic structure in all fast and moderate cooling rates. Only at a very slow cooling rate, does either alloy exhibit a slight increase in the transformation temperature due to a ferritic/bainitic transformation. However, the  $M_s$  temperature of the AerMet 100 alloy [498 K (225 °C)] is

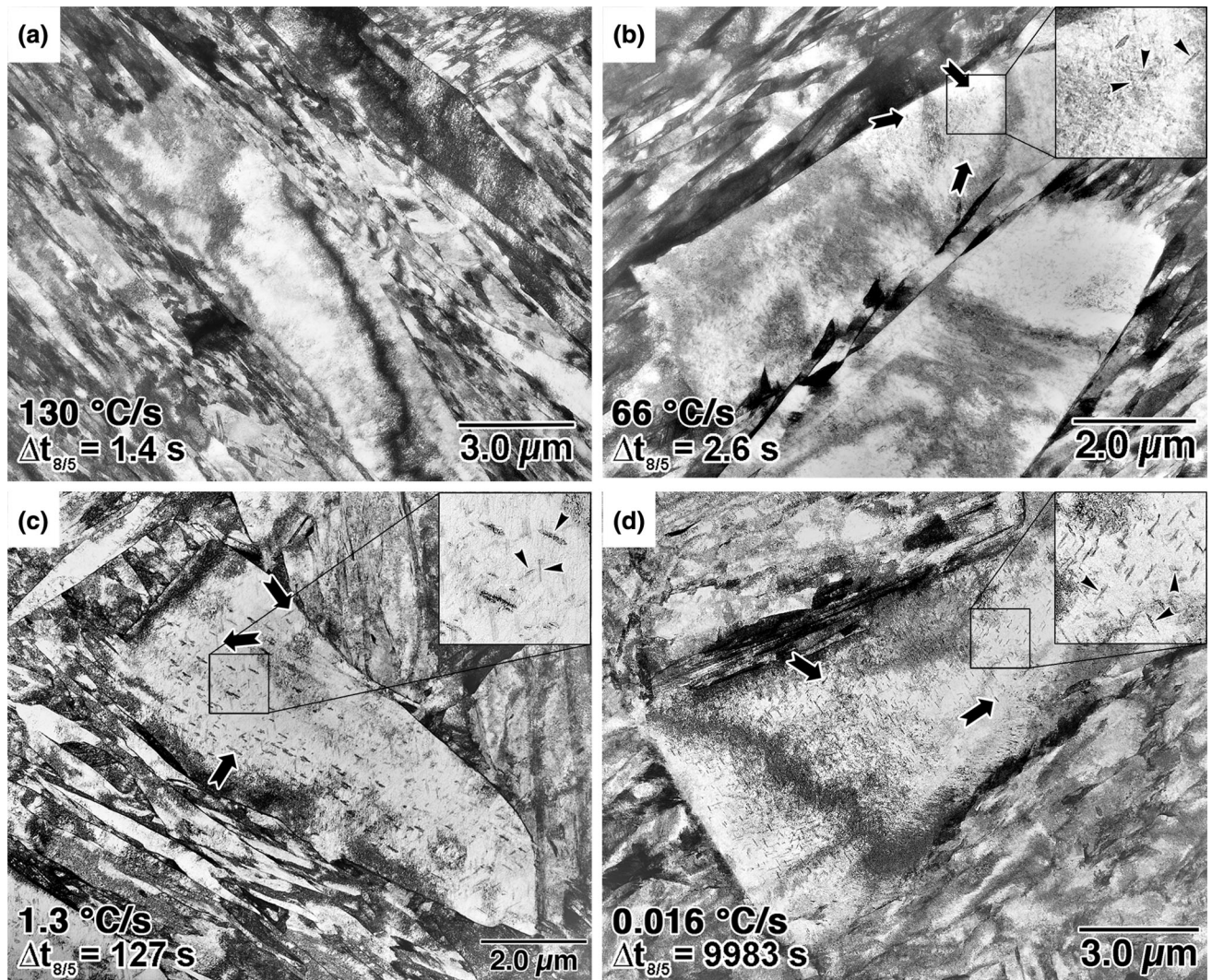


Fig. 6—TEM images of the microstructure as a function of cooling rate. (a)  $\Delta t_{8/5} = 1.4$  s (130 °C/s), (b)  $\Delta t_{8/5} = 2.6$  s (66 °C/s), (c)  $\Delta t_{8/5} = 127$  s (1.3 °C/s), and (d)  $\Delta t_{8/5} = 9983$  s (0.016 °C/s). Arrows indicate the cementite variants within the coarse martensite.

about 100 °C lower than that observed for the current alloy due to the differences in alloy composition.

#### IV. SUMMARY AND CONCLUSIONS

The microstructures, microhardness, and transformation behavior of a Fe-9Ni-0.11C alloy steel were characterized and used to construct a CCT diagram for this steel. These studies revealed that this steel has a very high hardenability and will produce a similar martensitic microstructure from the very fastest cooling rates examined ( $\Delta t_{8/5} = 1.4$  second, 130 °C/s) to cooling rates as slow as  $\Delta t_{8/5} = 994$  second (0.16 °C/s). The resultant microstructure is bimodal in nature, consisting of coarse autotempered martensite surrounded by fine laths of martensite. The coarse autotempered martensite contains multiple variants of carbide precipitates that develop at all but the fastest cooling rates.

At extremely slow cooling rates (those with  $\Delta t_{8/5} \geq 1991$  seconds or CR  $\leq 0.016$  °C/s), a fine lath ferrite microconstituent replaces the lath martensite observed at faster cooling rates.\* This ferritic microstructure

\*This microstructure is often sometimes referred to as ‘bainitic’ even though it is carbide free and thus does not develop through the concurrent precipitation of ferrite and carbide.

results in a decrease in the microhardness. In addition to the fine lath ferrite, the coarse martensite containing multiple carbide precipitate orientations is still observed.

Studies such as the experimental work presented here on the microstructural development and evolution during cooling of an Fe-9 pctNi steel are critical to providing not only an accurate understanding of microstructure evolution and phase stability in steels, but also to inform and validate predictive models of that

## ACKNOWLEDGMENTS

The authors would like to acknowledge the experimental assistance of Ed Pierpoint and many helpful discussions with Roy Vandermeer. We also gratefully acknowledge funding from the Office of Naval Research.

## REFERENCES

1. L.G. Kvidahl: *Weld. J.*, 1985, vol. 64 (7), pp. 42–48.
2. T.W. Montemarano, B.P. Sack, J.P. Gudas, M.G. Vassilaros, and H.H. Vanderveldt: *J. Ship Prod.*, 1986, vol. 2 (3), pp. 145–62.
3. T.L. Anderson, J.A. Hyatt, and J.C. West: *Weld. J.*, 1987, vol. 66 (9), pp. 21–26.
4. G.B. Olson: in *Proceedings of the 34th Sagamore Conference on Innovations in Ultrahigh Strength Steel Technology*, vol. 34, G.B. Olson, M. Azrin, and E.S. Wright, eds., 1987, pp. 3–66.
5. E.J. Czyryca, D.P. Kihl, and R. DeNale: *AMPTIAC Q.*, 2003, vol. 7 (3), pp. 63–70.
6. P.J. Konkol, K.M. Stefanick, and G.S. Pike: *Weld. J.*, 2011, vol. 90 (2), pp. 34–41.
7. W. Jolley: *JISI*, 1968, vol. 206, pp. 170–73.
8. W.C. Leslie, R.J. Sober, S.G. Babcock, and S.J. Green: *Trans ASM*, 1969, vol. 62, pp. 690–710.
9. G.R. Speich, D.S. Dabkowski, and L.F. Porter: *Metall. Trans.*, 1973, vol. 4, pp. 303–15.
10. C.D. Little and P.M. Machmeier: “Development of a Weldable High Strength Steel”: Report AFML-TR-75-148, US Air Force Materials Laboratory, Dayton, OH, 1975.
11. G. Dynamics: Patent Number 4,076,525, U.S., 1978.
12. P.M. Novotny and J.M. Dahl: *The 32nd Mechanical Working and Steel Processing Conference*, eds., Iron and Steel Society, 1991, pp. 275–81.
13. Y. Imai, Y. Tobe, K. Moriyama, S. Yano, S. Ueda, and S. Karino: United States Patent No. 4,814,141, March 1989.
14. X.J. Zhang and E.J. Czyryca: *Metallurgical Study of NS110B Steel (Part 2): Processing-Structure-Property Relations*, NSWCCD -61-TR-2003/06, May, 2003.
15. P.L. Harrison and R.A. Farrar: *Int. Mater. Rev.*, 1989, vol. 34 (1), pp. 35–51.
16. E.A. Wilson and S.H. Chong: *Metall. Mater. Trans. A*, 2002, vol. 33A, pp. 2425–31.
17. Carpenter Technology Corporation AerMet 100 Alloy Technical Datasheet. <http://cartech.ides.com/datasheet.aspx?i=103&e=161&c=techart&FMT=PRINT>. Accessed 22 Sept 2014.
18. S.H. Chong, A. Sayles, R. Keyse, J.D. Atkinson, and E.A. Wilson: *Mater. Trans. JIM*, 1998, vol. 39 (1), pp. 179–88.
19. K.W. Andrews: *JISI*, 1965, vol. 203, pp. 721–27.
20. W. Steven and A.G. Haynes: *JISI*, 1956, vol. 183, pp. 349–59.
21. H.W. Hayden, W.G. Moffatt, and J. Wulff: *The Structure and Properties of Materials, vol. III: Mechanical Behavior*, John Wiley & Sons, Inc., New York, 1965, p. 11.
22. X.J. Zhang: Unpublished Research; Private Communication, 2004.
23. R.A. Grange: *Met. Prog.*, 1961, vol. 70, pp. 73–75.
24. R.W. Fonda, G. Spanos, and R.A. Vandermeer: *Scripta Metall*, 1994, vol. 31, pp. 683–88.
25. G. Spanos, R.W. Fonda, R.A. Vandermeer, and A. Matuszeski: *Metall. Mater. Trans. A*, 1995, vol. 26, pp. 3277–93.
26. D.J. Rowenhorst, A. Gupta, C.R. Feng, and G. Spanos: *Scripta Mater.*, 2006, vol. 55 (1), pp. 11–16.
27. H.K.D.H. Bhadeshia, E. Keehan, L. Karlsson, and H.O. Andren: *Trans. Indian Inst. Met.*, 2006, vol. 59, pp. 689–94.
28. L.C. Chang and H.K.D.H. Bhadeshia: *Mater. Sci. Technol.*, 1996, vol. 12, pp. 233–36.



Fig. 7—TEM micrograph of the ferritic lath structure produced at a very slow cooling rate of  $\Delta t_{8/5} = 9983$  s (0.016 °C/s).

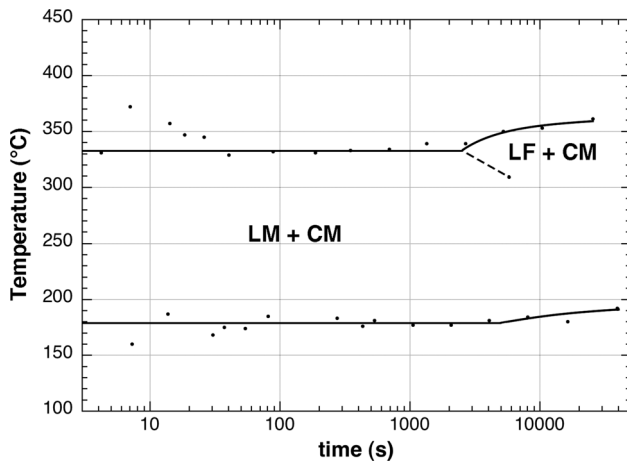


Fig. 8—Continuous cooling transformation diagram of this 0.09 pct C-10 pct Ni steel. LM = lath martensite; CM = coarse martensite; LF = lath (or bainitic) ferrite.

evolution (e.g., see<sup>[34–39]</sup>). Steel microstructures often contain a complex combination of constituents with similar appearances, often requiring multiple complementary analytical techniques for an accurate identification. In addition, the properties of these steels are directly dependent on the volume fraction, distribution, morphology, and identity of those constituents. It is, therefore, essential to acquire experimental data such as this to enable the development and validation of predictive models, thereby expediting new alloy and product development cycles through the promising

29. E. Keehana, L. Karlsson, H.K.D.H. Bhadeshia, and M. Thuvander: *Mater. Charact.*, 2008, vol. 59, pp. 877–82.
30. R.W. Fonda and G. Spanos: *Metall. Mater. Trans. A*, 2000, vol. 31A, pp. 2145–53.
31. G. Krauss: *Steels: Processing, Structure, and Performance*, ASM International, Materials Park, OH, 2005, pp. 82, 343.
32. M. Katsumata, O. Ishiyama, T. Inoue, and T. Tanaka: *Mater. Trans. JIM*, 1991, vol. 32 (8), pp. 715–28.
33. S. Zajac, V. Schwinn, and K.-H. Tacke: *Mater. Sci. Forum*, 2005, vols. 500–501, pp. 387–94.
34. H.I. Aaronson: in *The Decomposition of Austenite by Diffusional Processes*, V.F. Zackay and H.I. Aaronson, eds., Interscience, New York, 1962, pp. 387–546.
35. M. Hillert: in *The Decomposition of Austenite by Diffusional Processes*, V.F. Zackay and H.I. Aaronson, eds., Interscience, New York, 1962, pp. 197–237.
36. T. Tanaka, H.I. Aaronson, and M. Enomoto: *Metall. Mater. Trans. A*, 1995, vol. 26A, pp. 535–45.
37. G.B. Olson: *Science*, 1997, vol. 277 (5330), pp. 1237–42.
38. G. Spanos, A.B. Geltmacher, A.C. Lewis, J.F. Bingert, M. Mehl, D. Papaconstantopoulos, Y. Mishin, A. Gupta, and P. Matic: *Mater. Sci. Eng. A*, 2007, vols. 452–453, pp. 558–68.
39. A.C. Lewis, K. Jordan, and A.B. Geltmacher: *Metall. Mater. Trans. A*, 2008, vol. 39A, pp. 1109–17.
40. J. Allison, M. Li, C. Wolverton, and X.M. Su: *JOM*, 2006, vol. 58, pp. 28–35.
41. *Integrated Computational Materials Engineering: A Transformational Discipline for Improved Competitiveness and National Security*, The National Academies Press, Washington, DC, 2008.
42. *Integrated Computational Materials Engineering (ICME): Integrating ICME in The Automotive, Aerospace, and Maritime Industries*, The Minerals, Metals and Materials Society (TMS), Warrendale, PA, 2013.
43. M. Li, C. Campbell, K. Thornton, E. Holm, and P. Gumbsch, eds.: *Proceedings of the 2nd World Congress on Integrated Computational Materials Engineering (ICME)*, John Wiley & Sons, Inc., Hoboken, NJ, 2013.